

**Progress Report
for the Stardust Isotope Group**

**MPI for Chemistry Mainz
(P. Heck, P. Hoppe, J. Huth)**

June 16, 2006

**NanoSIMS C-, N-, and O-isotopic analyses
of residues in large craters in Al foils**

**C2013N
C2086N**

Samples

Residues in two large craters in Al foils C2013N (#LC1) and C2086N (#LC2) were studied for O- (both craters) and C- and N-isotopic compositions (so far only #LC1). Sizes of #LC1 and #LC2 are 140 μm and 59 μm , respectively (Fig. 1). Prior to the NanoSIMS measurements both samples were characterized by EDX scanning (#LC1: done at Mainz, see our progress report to Cratering Group of June 15, 2006; #LC2: done at NHM, see progress report by Anton Kearsley of May 2006). The main purpose of the C-, N-, and O-isotopic analyses on these Stardust samples was to find presolar materials. While presolar (stardust) grains can be recognized by large O- or C-isotopic anomalies, presolar molecular cloud material is characterized by large ^{15}N (and D) enrichments.

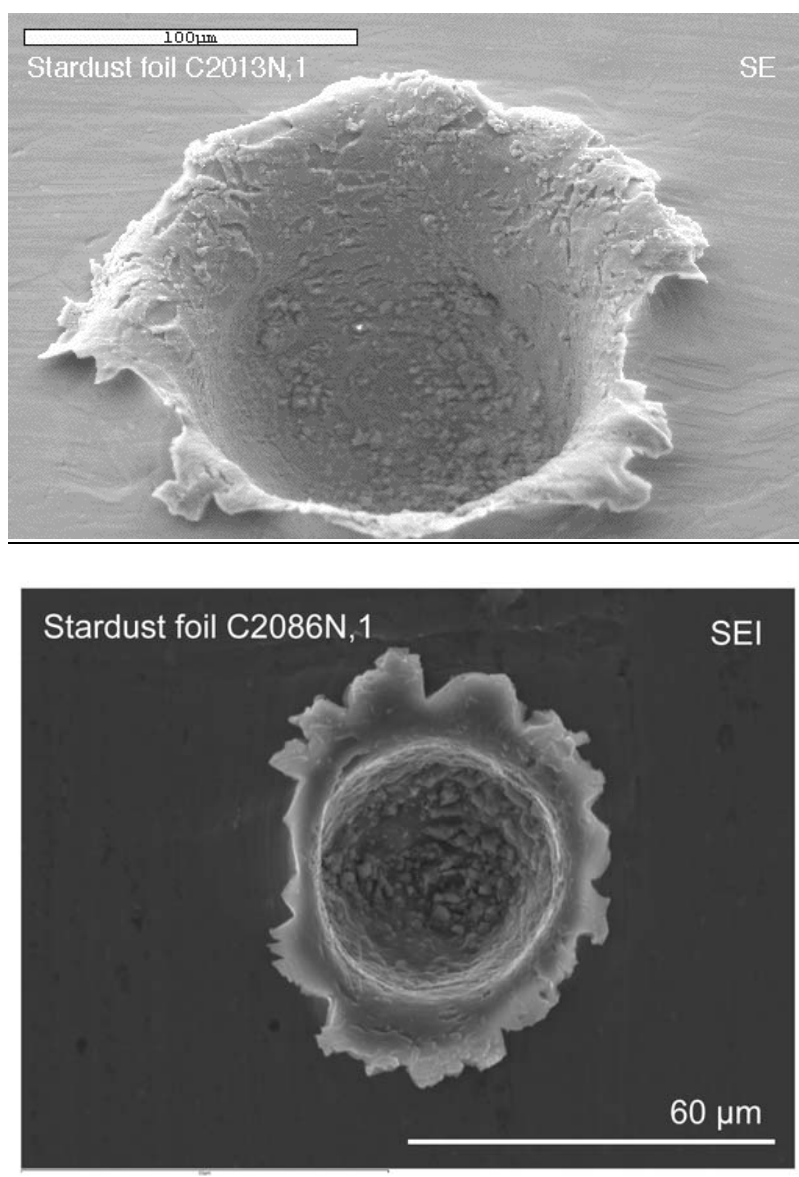


Figure 1: SEM images of large craters in Al foils C2013N (top, “#LC1”) and C2086N (bottom, “#LC2”; picture taken by Anton Kearsley).

O-isotopic measurements

The data are summarized in Table 1. The isotope measurements (all three O isotopes along with ^{28}Si and AlO) were made on material both from the crater lip and crater floor. Selected ion images are shown in Figs. 2 and 3. In total, one area with size $30 \times 30 \mu\text{m}^2$ (#LC1) and 50 (#LC1) and, respectively, 35 (#LC2) areas with sizes of $10 \times 10 \mu\text{m}^2$ were investigated. Automated particle recognition routines identified some 3600 (#LC1) and 2400 (#LC2) O-rich grains/subareas in the ion images. For all of these particles O-isotopic ratios were calculated (normalized to the averages of $^{17}\text{O}/^{16}\text{O}$ and $^{18}\text{O}/^{16}\text{O}$ ratios in each area). The data are displayed in Figs. 4 and 5. We consider a particle as a presolar grain candidate if (i) $\delta^{17}\text{O}$ or $\delta^{18}\text{O}$ is $>200 \text{ ‰}$ or $< -200 \text{ ‰}$ and (ii) the anomaly is larger than 4σ (based on the counting statistical error plus systematic uncertainty due to crater topography which was estimated to be $\sim 50 \text{ ‰}$ ($\delta^{17}\text{O}$) and $\sim 20 \text{ ‰}$ ($\delta^{18}\text{O}$) for #LC1 and, respectively, $\sim 70 \text{ ‰}$ ($\delta^{17}\text{O}$) and $\sim 35 \text{ ‰}$ ($\delta^{18}\text{O}$) for #LC2). A 3σ criterion is not sufficient because with the number of particles considered here several grains will fall outside this limit, simply for statistical reasons. The σ deviations for grains with $\delta^{17}\text{O} > 200 \text{ ‰}$ and $< -200 \text{ ‰}$ are plotted in Figs. 6 and 7. There are a few grains outside the 3σ limit but no grain plots outside the 4σ limit. In Fig. 8 the O-isotopic ratios are plotted along with those of presolar silicate grains from the Acfer 094 meteorite, most of which exhibit enrichments in ^{17}O by more than a factor of 2. Given the O-isotopic signatures of presolar silicates and the statistics of O-isotopic ratios of the grains studied here none of them can be considered as of presolar origin.

If we consider the typical size of presolar silicates and compare the area of one presolar silicate ($d = 300 \text{ nm}$) with the total area of recognised O-rich particles in #LC1 and #LC2 then we obtain an upper limit for the abundance of presolar O-rich grains of 39 ppm. A proper estimate for the presolar grain abundance is based on the assumption that the material did not melt so that localized presolar signatures are still recognisable. If this is not the case then the upper limit for the abundance estimate will be higher.

Table 1: Summary of O-isotopic measurements on #LC1 and #LC2 residues.

Crater residue	Analyzed area (μm^2)	Recognized particles	Particle area (μm^2)	Average error $^{17}\text{O}/^{16}\text{O}$ ¹	Average error $^{18}\text{O}/^{16}\text{O}$ ¹	Presolar grains?
#LC1	5900	3640	1356	97 ‰	42 ‰	no
#LC2	3500	2409	955	97 ‰	41 ‰	no
Total	9400	6049	2311	97 ‰	42 ‰	$<39 \text{ ppm}^2$

¹Per particle; based on counting statistics.

²Corresponds to the abundance of one presolar grain with size of 300 nm.

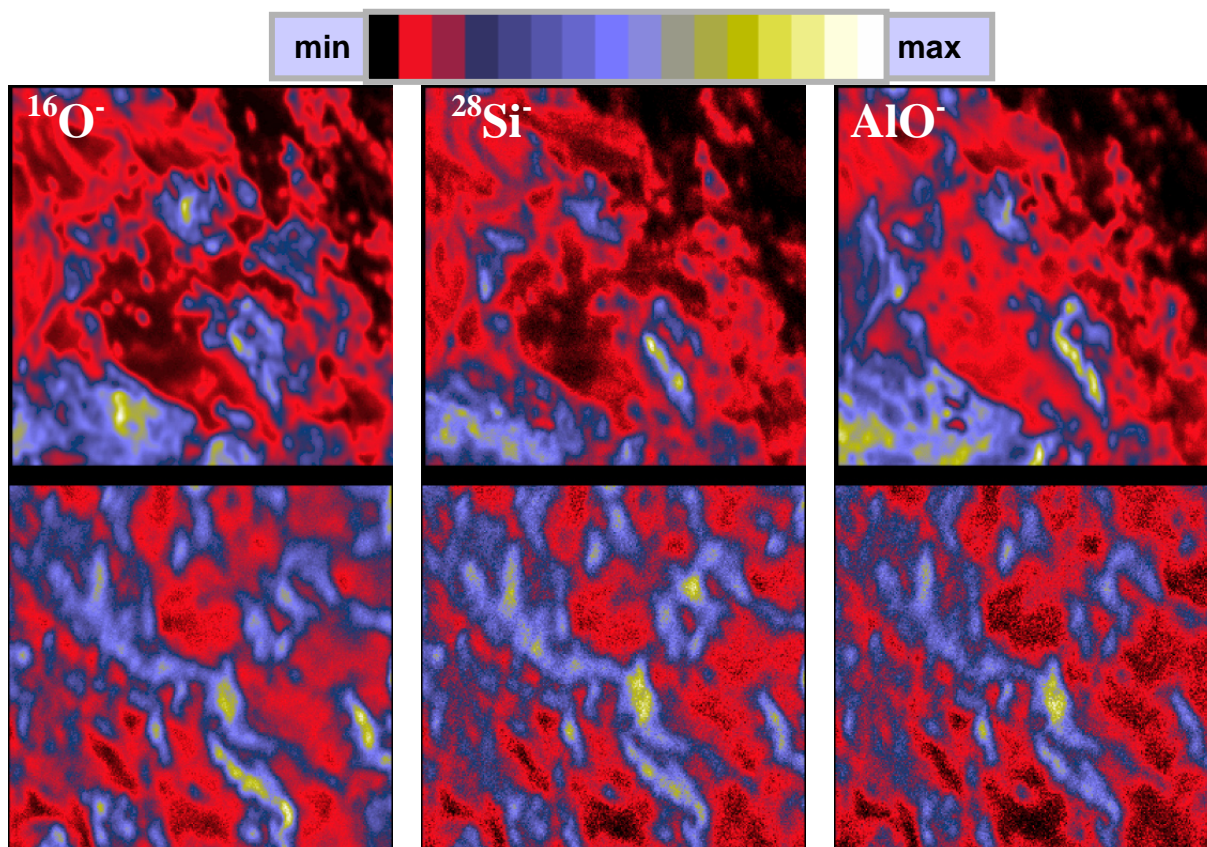


Figure 2: Ion images of $^{16}\text{O}^-$, $^{28}\text{Si}^-$, and AlO^- for #LC1 residue on crater lip (top row) and floor (lower row). Field of view is $10 \times 10 \mu\text{m}^2$.

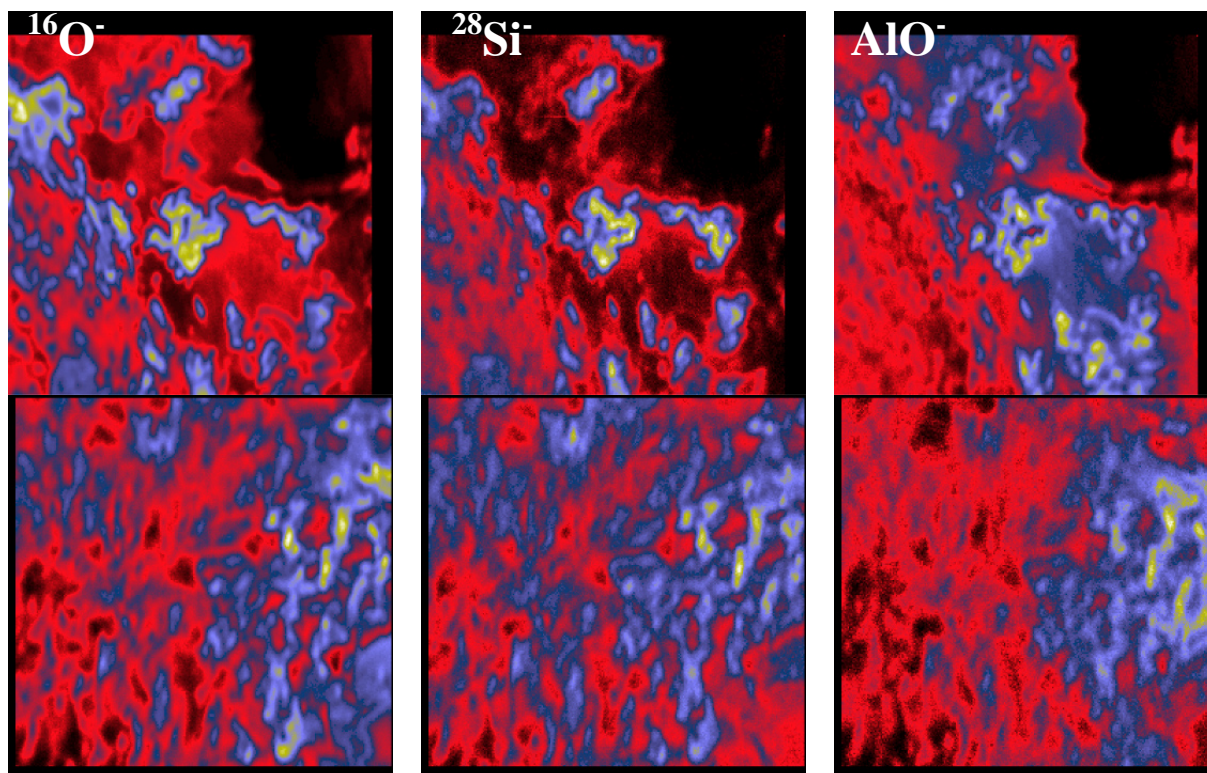


Figure 3: Ion images of $^{16}\text{O}^-$, $^{28}\text{Si}^-$, and AlO^- for #LC2 residue on crater lip (top row) and floor (lower row). Field of view is $10 \times 10 \mu\text{m}^2$.

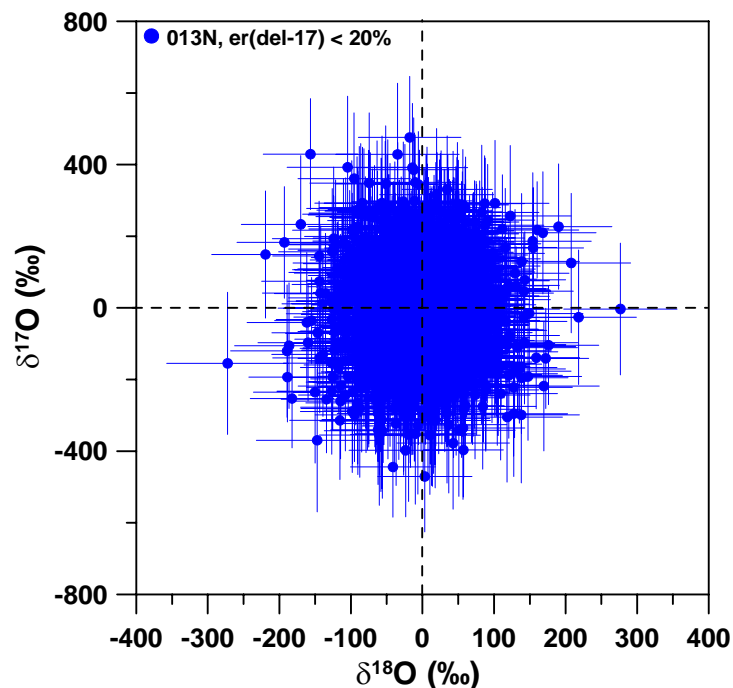


Figure 4: O-isotopic compositions of O-rich particles in crater #LC1 (C2013N). Only data of grains with error in $\delta^{17}\text{O}$ of $< 20\%$ are shown. No QSA correction (calculated to be only 6 ‰ on average) was made. Errors are 1σ .

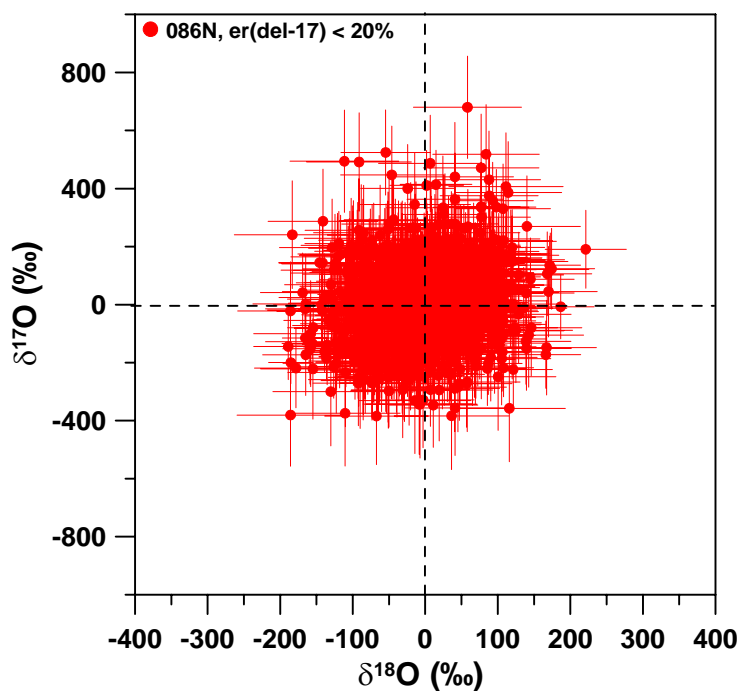


Figure 5: O-isotopic compositions of O-rich particles in crater #LC2 (C2086N). Only data of grains with error in $\delta^{17}\text{O}$ of $< 20\%$ are shown. No QSA correction (calculated to be only 6 ‰ on average) was made. Errors are 1σ .

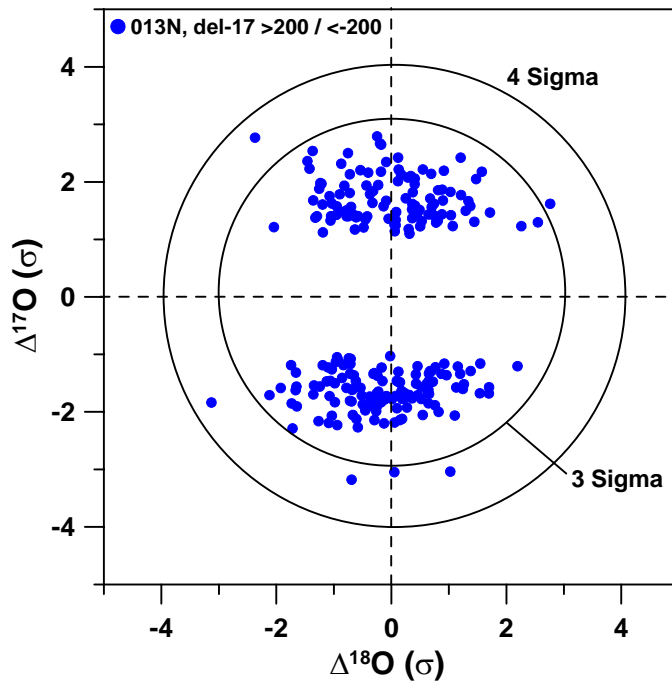


Figure 6: Sigma deviations of O-isotopic ratios of O-rich particles in crater #LC1 (C2013N). Only data of grains with $\delta^{17}\text{O} > 200$ ‰ and $\delta^{17}\text{O} < -200$ ‰ are shown. No grains plot outside the 4 sigma limit.

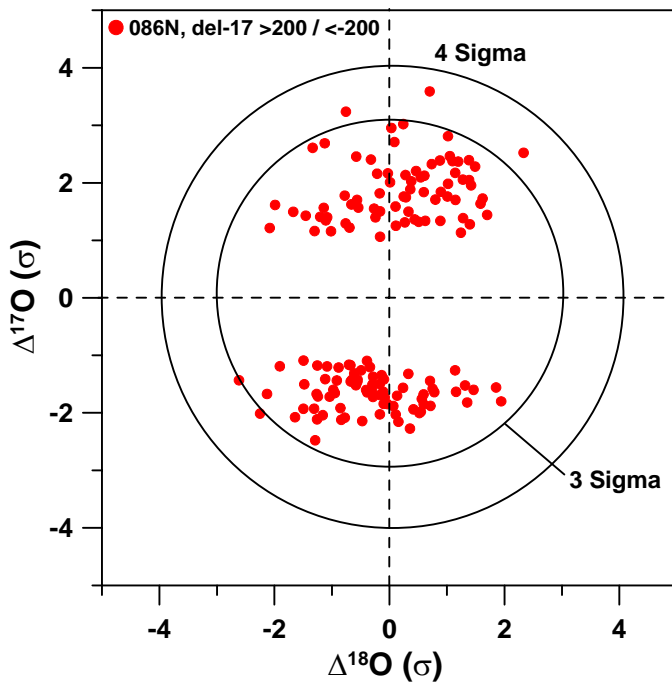


Figure 7: Sigma deviations of O-isotopic ratios of O-rich particles in crater #LC2 (C2086N). Only data of grains with $\delta^{17}\text{O} > 200$ ‰ and $\delta^{17}\text{O} < -200$ ‰ are shown. No grains plot outside the 4 sigma limit.

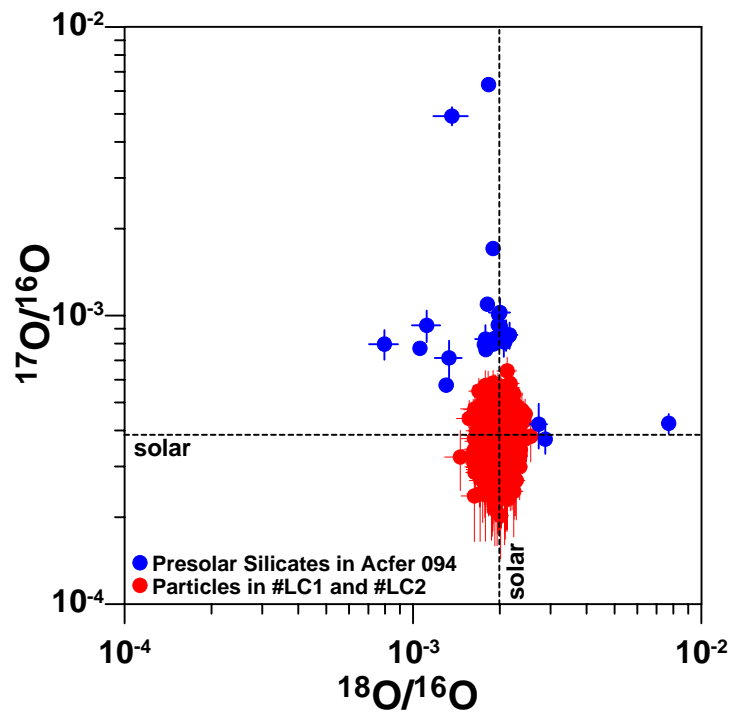


Figure 8: O-isotopic compositions of individual particles in craters #LC1 and #LC2. Data for presolar silicates from the Acfer 094 meteorite are shown for comparison. Errors are 1σ .

C- and N-isotopic measurements

For the C- and N-isotopic measurements negative secondary ion images of ^{12}C , ^{13}C , $^{12}\text{C}^{14}\text{N}$, $^{12}\text{C}^{15}\text{N}$, and ^{28}Si were acquired for 17 regions on the lip of crater #LC1, each $10 \times 10 \mu\text{m}^2$ in size (Fig. 9 shows an example). Thorough cleaning prior to the isotope measurements was required to remove C- and N-rich contamination on the surface. C- and N-isotopic data were normalized to measurements on nearby C- and N-rich contamination on the Al foil ($^{13}\text{C}/^{12}\text{C} = 0.0113$, $^{15}\text{N}/^{14}\text{N} = 0.00346$). On several areas we observed a strong $^{11}\text{B}^{16}\text{O}$ signal (possibly contamination from the glass container which was used for the foil shipment). The $^{11}\text{B}^{16}\text{O}$ peak can not be fully separated from the $^{12}\text{C}^{15}\text{N}$ peak. To avoid potential contributions from this interference to the $^{12}\text{C}^{15}\text{N}$ signal, the measurements in 11 regions were done at the left side of the $^{12}\text{C}^{15}\text{N}$ peak. The N data from the remaining 6 regions are not considered here. A test measurement on one of the surface contamination areas rich in C and N, where $^{11}\text{B}^{16}\text{O}$ was exceptionally high ($^{11}\text{B}^{16}\text{O}/^{13}\text{C}^{14}\text{N} \sim 9$, i.e. $^{11}\text{B}^{16}\text{O}/^{12}\text{C}^{15}\text{N} \sim 27$ for isotopically normal N), yielded a normal $^{15}\text{N}/^{14}\text{N}$ ratio, as expected.

Some 440 nitrogen-rich grains/subareas in crater #LC1 were identified by an automated particle recognition routine. Their nitrogen turned out to be isotopically heavy (Fig. 10). The average $\delta^{15}\text{N}$ of these N-rich particles is $+451 \pm 7 \text{‰}$, the average $\delta^{13}\text{C}$ is $-25 \pm 1 \text{‰}$ (the errors are based on counting statistics). The whole analyzed crater area has $\delta^{15}\text{N} = +330 \pm 4 \text{‰}$ and $\delta^{13}\text{C} = -20 \pm 1 \text{‰}$. In local subareas $\delta^{15}\text{N}$ sometimes reach 1000‰ (Fig. 10). This signature is similarly observed in some IDPs and in insoluble organic matter from carbonaceous chondrites. Nitrogen is not well correlated with the distribution of C but seems to follow more closely the distribution of Si (see Fig. 9). It appears that much of the C is still contamination while N may be present in tiny (C-rich?) inclusions within the Si-rich material. Our data contrast with the results obtained for microtome sections 2-1-8-C/D which have very low N concentrations and where no N-isotope anomalies ($^{15}\text{N}/^{14}\text{N}$ ratios are normal within a few percent) have been found (see our progress report of April 26, 2006).

In a next step we will study the C- and N-isotopic compositions in the residue of crater #LC2. It will be interesting to see whether we will be able to confirm the results found for #LC1 or whether #LC2 has a distinct N-isotopic signature.

Stardust grains, such as presolar SiC and graphite, were not found in the 17 regions analyzed (Table 2). None of the 687 C-rich particles/subareas identified by automated particle recognition has a $^{13}\text{C}/^{12}\text{C}$ ratio that deviates more than 20 % and more than 4σ from the solar ratio. If we take the area of C-rich particles analyzed here then one presolar carbonaceous grain with size of 300 nm would represent an abundance of 332 ppm; this can be considered as an estimate for an upper limit for the abundance of presolar carbonaceous grains.

Table 2: Summary of C-isotopic measurements on C-rich grains in the #LC1 residue.

Grain mode	Analyzed area (μm^2)	Recognized particles	Particle area (μm^2)	Average error ¹ $^{13}\text{C}/^{12}\text{C}$	Presolar grains? Abundance upper limit ²
C	1700	687	271	33 ‰	no < 332 ppm

¹Per particle; based on counting statistics.

²Corresponds to the abundance of one presolar grain with size of 300 nm.

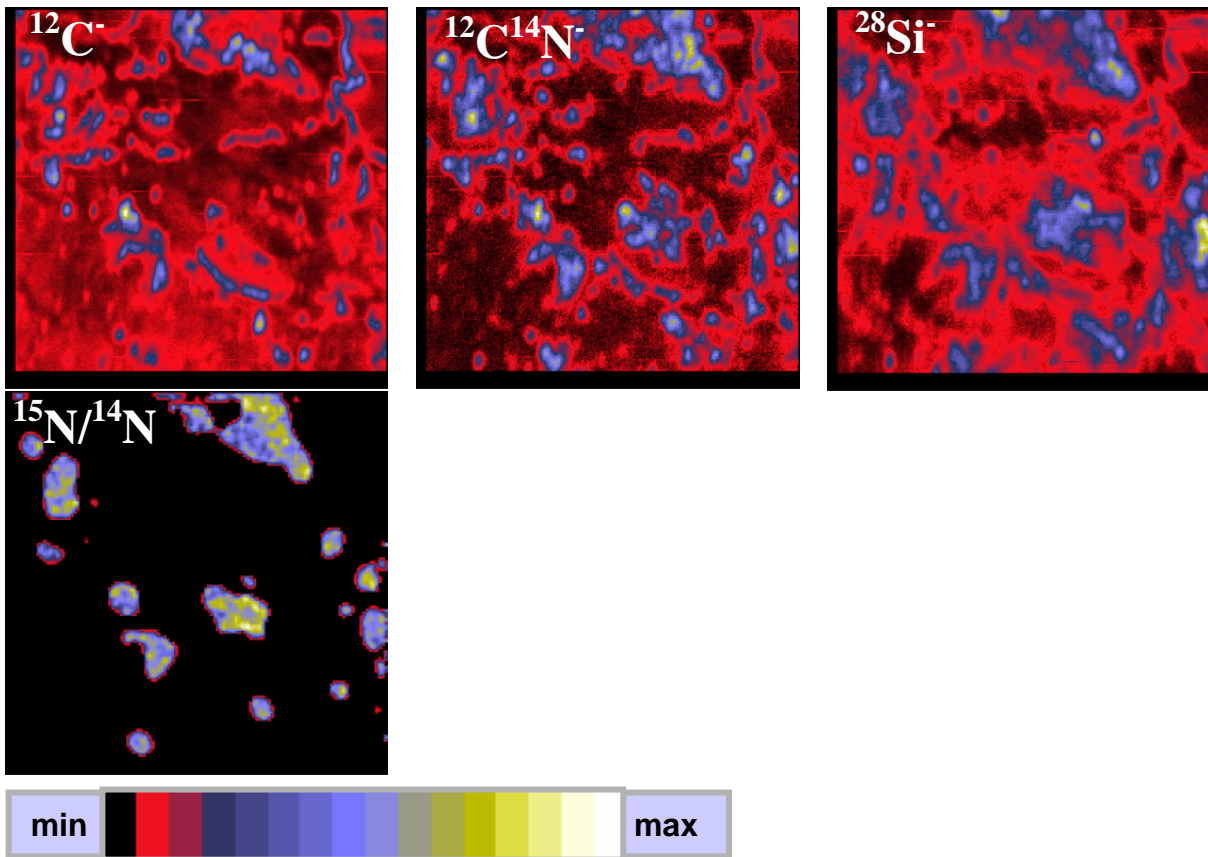


Figure 9: NanoSIMS ion images of ^{12}C , $^{12}\text{C}^{14}\text{N}$, ^{28}Si , and $^{15}\text{N}/^{14}\text{N}$ (from $^{12}\text{C}^{15}\text{C}^-/^{12}\text{C}^{14}\text{N}^-$) in a $10 \times 10 \mu\text{m}^2$ -sized subarea of crater #LC1 (C2013N). Nitrogen is heavily enriched in ^{15}N in several subareas (yellow in the $^{15}\text{N}/^{14}\text{N}$ image).

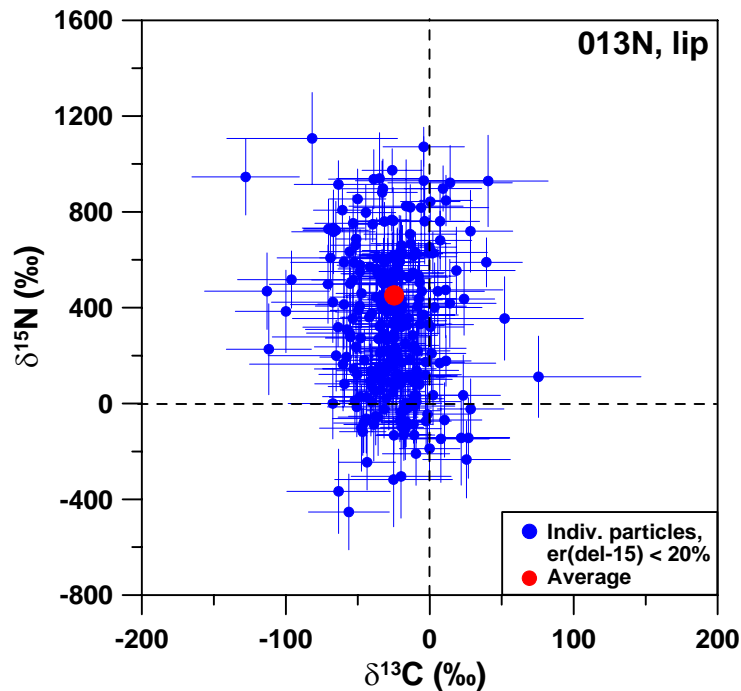


Figure 10: C- and N-isotopic compositions of individual N-rich particles/subareas (blue) and of their averages (red) in crater #LC1 (C2013N). Only data points with error of less than 200 ‰ in $\delta^{15}\text{N}$ are shown.